BIOCHEMISTRY

 Volume 46, Number 24 June 19, 2007

Articles

Amyloid Formation via Supramolecular Peptide Assemblies†

Roger A. Moore,‡ Stanley F. Hayes,§ Elizabeth R. Fischer,§ and Suzette A. Priola*,‡

Laboratory of Persistent Viral Diseases and Microscopy Unit, Research Technologies Section, RTB, Rocky Mountain Laboratories, National Institute of Allergy and Infectious Disease, National Institutes of Health, 903 South 4th Street, Hamilton, Montana 59840

Received February 5, 2007; Revised Manuscript Received March 29, 2007

ABSTRACT: Amyloid fibrils have been classically defined as linear, nonbranched polymeric proteins with a cross β-sheet structure and the ability to alter the optical properties of the amyloid-specific dye Congo Red. Mounting evidence suggests that soluble oligomeric peptide assemblies ~2-20 nm in diameter are critical intermediates in amyloid formation. Using a pathogenic prion protein peptide comprised of residues 23−144, we demonstrate that, under quiescent but not agitated conditions, much larger globular assemblies up to 1 μm in diameter are made. These globules precede fibril formation and directly interact with growing fibril bundles. Fibrils made via these large spherical peptide assemblies displayed a remarkable diversity of ultrastructural features. Fibrillization of the Aβ1−40 peptide under similar conditions yielded similar results, suggesting a mechanism of general amyloid formation that can proceed through intermediates much larger than those previously described. Our data suggest that simply changing the physical microenvironment can profoundly influence the mechanism of amyloid formation and yield fibrils with novel ultrastructural properties.

Amyloid formation is an incompletely understood process. However, the biological relevance of amyloid is underscored by the identification of more than 20 different human disorders involving abnormal amyloid deposition (*1*), including prion diseases such as Gerstmann-Sträussler-Schienker syndrome (GSS)[1] and Alzheimer's disease (AD). Several mechanisms have been proposed for the formation of amyloid fibrils, most of which are consistent with partially unfolded protein molecules slowly self-aggregating into small oligomeric nuclei which then propagate more rapid fibril growth (*1*, *2*). The use of in vitro models to understand the mechanistic processes leading to amyloid fibrils has been well-validated (*3*, *4*) but is complicated by the many variables that influence fibrillization and the diversity of the observed prefibrillar species. The extent to which these various aggregates, oligomers, and apparent protofibrils represent productive reaction intermediates is often unclear, since off-pathway oligomeric species have also been reported (*5*−*7*).

Many researchers have reported that soluble oligomers ~2−20 nm in diameter are key amyloidogenic intermediates and are largely responsible for the pathology associated with amyloidoses such as GSS and AD (*8*−*13*). These well-

† This research was supported by the intramural research program of the National Institute of Allergy and Infectious Disease, National Institutes of Health.

* To whom correspondence should be addressed. Telephone: (406) 363-9319. Fax: (406) 363-9286. E-mail: spriola@nih.gov.

‡ Laboratory of Persistent Viral Diseases.

§ Microscopy Unit, Research Technologies Section, RTB.

[1] Abbreviations: GSS, Gerstmann-Sträussler-Scheinker syndrome; AD, Alzheimer's disease; PrP, prion protein; HaPrP23−144, hamster PrP peptide with a stop codon at residue 145; Aβ40, Alzheimer's Aβ1−40 peptide; ATR-FTIR, attenuated total reflectance Fourier transform infrared spectroscopy; TEM, transmission electron microscopy; HD, hanging drop; ThT, thioflavin T; SEM, scanning electron microscopy; Aβ42, Alzheimer's Aβ1−42 peptide.

10.1021/bi700247y CCC: $37.00
Published on Web 05/24/2007

documented small oligomers have exhibited diverse morphologies when visualized by electron and atomic force microscopy (*14*−*20*), suggesting that fibrillization reactions may proceed through multiple reaction pathways. Indeed, it has been demonstrated that variations in growth conditions for a specific peptide can impact the underlying molecular structure of the amyloid itself (*21*).

Amyloid can accumulate in various tissues (*1*), often with distinctive histopathological features (*22*). It is therefore probable that environmental variables directly influence the pathway of assembly, the mechanism, and the underlying molecular structure of the resulting amyloid. To determine the effects of the physical environment upon key mechanistic aspects of amyloidogenesis, we compared fibrillization via either agitation in microcentrifuge tubes or hanging drop vapor diffusion. Hanging drop vapor diffusion is used extensively for protein crystallization and provides a static, low-convection environment with a markedly increased hydrophobic air−buffer interface area compared to that of the microcentrifuge tube environment. As a model amyloid forming peptide, we first used a hamster prion protein peptide containing a stop codon at position 145, HaPrP23−144. In humans, this peptide is the result of a stop codon at position 145 of the *Prnp* gene, resulting in a form of cerebral amyloid angiopathy with significant perivascular accumulation of PrP amyloid in the brain (*23*). As a second model peptide, Aβ1−40 (Aβ40), which is associated with AD, was studied.

Our results show that amyloid formation in the static hanging drop environment is closely associated with the formation of peptide globules up to 1 μm in size. Closer analysis of the fibrillization kinetics demonstrated that such large globules preceded the formation of amyloid in the hanging drop environment, suggesting an intermediary role for these structures. This mechanism was markedly different from that observed in the agitated microenvironment where fibril formation was consistent with progression via smaller oligomeric intermediates. The amyloid formed in these two systems was morphologically and structurally different, suggesting that contrasting fibrillization environments can trigger different mechanisms leading to distinct types of amyloid.

EXPERIMENTAL PROCEDURES

Purification and Fibrillization of HaPrP23−*144.* HaPrP23−144 from sequenced DNA was purified from *Escherichia coli* Rosetta cells as described previously (*24*) and kept at 4 °C either in water (∼0.1 mg/mL) or as a lyophilized powder. The purity of the peptide was assessed by SDS−PAGE, Western blotting, and MALDI to be >99% (data not shown). Fibrillization reactions were initiated after dialysis against glass-distilled milliQ water (16 L). The peptide was then sterile filtered and concentrated by ultrafiltration (Amicon, MWCO of 5000) to 125 μM with water. Buffer concentrations were adjusted to 10 mM from a 1 M stock of the appropriate buffer as stated in the figure legends. The time course reactions for both hanging drop and agitated samples were conducted in 10 mM Bis-Tris propane (pH 7.0) after ultracentrifugation (256000*g*) for 30 min to remove protofibrils or aggregated material. Selected reaction mixtures were agitated in an Eppendorf Thermomixer at 1000 rpm with a 500 μL volume in siliconized microfuge tubes (VWR). Hanging drops (HDs) were set up in pregreased VDX plates (Hampton Research) on a siliconized glass coverslip with 10 μL over a 900 μL reservoir solution containing 50 mM of the same sterile-filtered buffer at 20 °C. Analysis of the fibrillization reactions by ThT was performed as described previously (*24*).

Fibrillization of Aβ40. Lyophilized Aβ40 (0.5 mg) from rPeptide (Bogart, GA) was reconstituted in 1% ammonium hydroxide (2 mL) and subjected to ultracentrifugation (256000*g*). This solution was adjusted to 25 mM MES (pH 5.4) and then either shaken at 600 rpm and 37 °C or suspended in hanging drops on a siliconized glass slide over 1 mL of 125 mM MES (pH 5.4) in a 24-well VDX tray.

Transmission Electron Microscopy. Sample suspensions (5 μL) were diluted 10-fold with reaction buffer and settled on Parlodian- or Formvar-coated copper grids. After excess fluids were micropipetted from the grid surface, the grid was washed with water and stained for 60 s with 0.3% aqueous uranyl acetate. Excess stain was removed, and the samples were dried at room temperature. The samples were analyzed at 80 kV in a Hitachi 7500 electron microscope or 60 kV on a Philips CM-10 (FEI, Hillsboro, OR) transmission electron microscope. Digital images were captured with an AMT digital camera system (AMT, Chazy, NY).

Extensive control studies were also performed with the different reaction buffers and uranyl acetate but excluding the peptide. No fibrillar structures were observed in any of these preparations (e.g., Figure 1A inset), indicating that the contribution of a TEM artifact from different reaction buffers (e.g., Tris vs Hepes) was unlikely. For direct comparisons between the agitated and HD preparations, the buffer and the uranyl acetate used for staining procedures were kept constant, minimizing any potential structural differences due to sample preparation.

Congo Red Staining and Polarized Light Microscopy. The fibrillization reaction mixture (5 μL) was applied to a glass slide, treated with 4 μL of a 0.2% Congo Red/ethanol solution (Sigma), and dried in air for 6 h. The suspension was then washed three times with 95% ethanol and dried with a stream of nitrogen. The sample was observed under bright field illumination and then between crossed polars at 40× magnification using a Zeiss HB50 polarizing microscope equipped with a digital camera. No birefringence was observed in buffer samples that did not contain HaPrP23−144 (data not shown).

Scanning Electron Microscopy. Droplets (5 μL) of sample in suspension were allowed to settle for 20 min on silicon chips and fixed with a 2.5% glutaraldehyde/4% paraformaldehyde mixture in 0.1 M sodium cacodylate buffer for 30 min. Samples were postfixed by alternating two rounds of 15 min in a 1% OsO_4/0.8% $K_4Fe(CN)_6$ mixture and 30 min in 1% tannic acid. Samples were dehydrated in ethanol and critical point dried in a Bal-Tec, cpd 030 drier (Balzers, Liechtenstein). Chips were mounted on aluminum studs (Ted Pella, Inc., Redding, CA), coated with 25 Å of chromium for HaPrP23−144 samples or 25 Å of platinum for Aβ40 samples in an IBS/TM200S ion beam sputterer (South Bay Technology, Inc., San Clemente, CA), and viewed at 5−30 kV with an S-5200 in-lens electron microscope in secondary mode (Hitachi, Tokyo, Japan). Digital images were processed

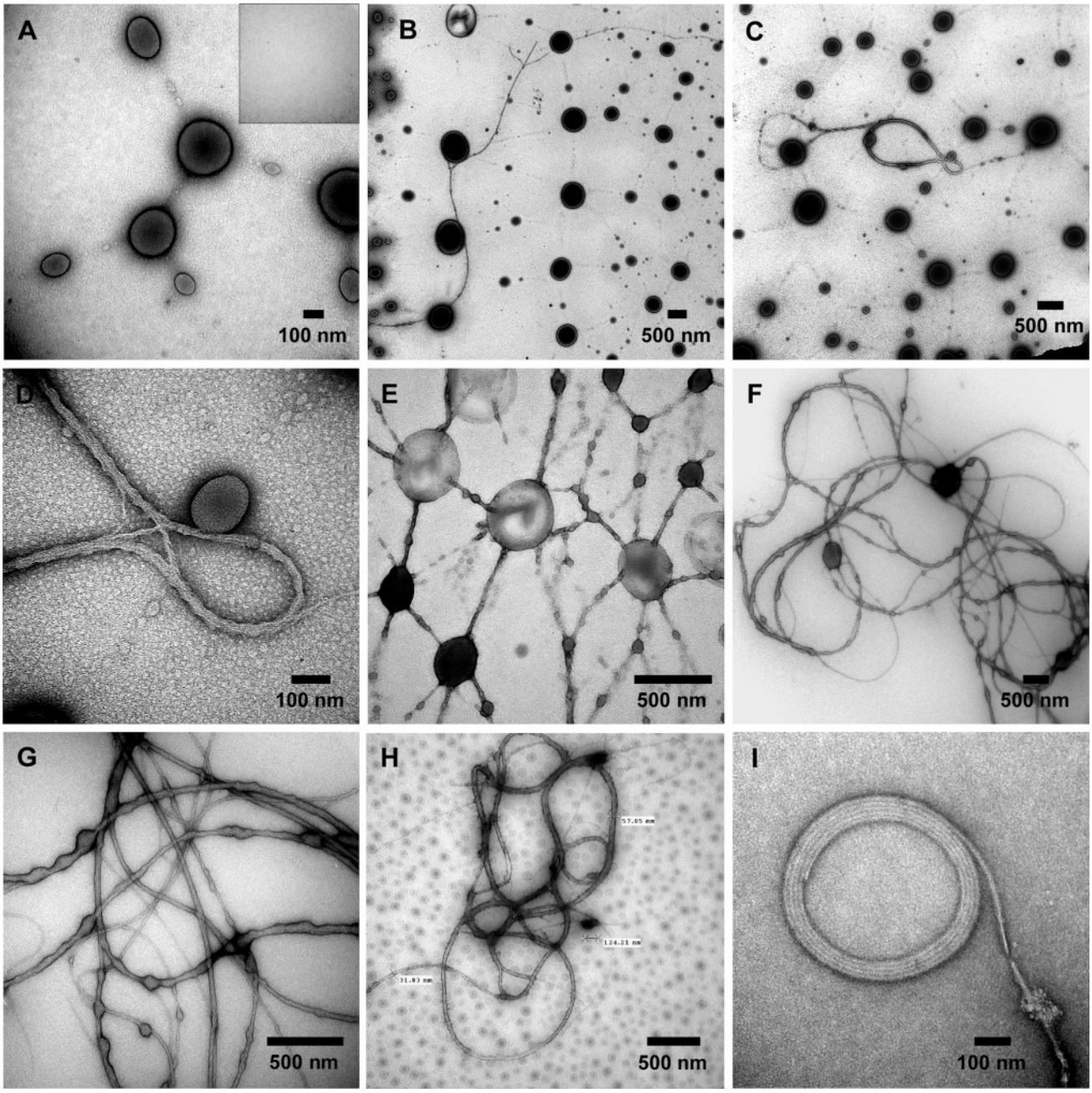

FIGURE 1: Transmission electron microscopy of HaPrP23−144 globules and fibrils from hanging drops at neutral to basic pH under nondenaturing conditions. Hanging drops (10 μL) on glass coverslips were composed of 125 μM HaPrP23−144 in 10 mM buffer over a 50 mM reservoir solution of the same buffer in a 24-well VDX plate incubated at 20 °C under the following conditions: (A) potassium phosphate (pH 7.4) (inset, image of buffer without peptide), (B and C) Bis-Tris propane (pH 7.0), (D) a-higher magnification image of the fibrillar bundle in panel C, (E) Bicine (pH 7.4), (F and G) HEPES (pH 7.5), and (H) Tris (pH 8.5). The boxed numbers represent measurements for, clockwise from top, the width of a fibril bundle (57.05 nm), the distance between two globules (124.21 nm), the width of a fibril bundle (31.83 nm). (I) Bicine (pH 7.4).

with Adobe Photoshop, version 7.0 (Adobe Systems, Mountain View, CA).

Attenuated Total Reflectance Fourier Transform Infrared Spectroscopy (ATR-FTIR). Agitated and hanging drop reaction mixtures were pelleted by centrifugation (14000 rpm). Agitated fibril pellets containing ≥80% of the total protein were deposited on the diamond surface of the instrument as aqueous slurries and dried with a stream of anhydrous nitrogen gas. Only a relatively small percentage (≤20%) of the original HaPrP23−144 in hanging drop reaction mixtures could be isolated by centrifugation, and it was often difficult to identify a discernible pellet. However, a fibril-enriched portion, or "soft pellet", was used for ATR-FTIR analyses, which were performed as described previously (*24*).

RESULTS

HaPrP23−144 Forms Large Globular Assemblies. Highly purified HaPrP23−144 was fibrillized under either agitated or hanging drop (HD) conditions and analyzed by transmission electron microscopy (TEM). No fibrils were observed in buffer alone (Figure 1A, inset) or in a mock purification in which an empty vector was transformed into *E. coli* (Figure 1A of the Supporting Information). However, when HaPrP23−144 was suspended in HDs without detergents or

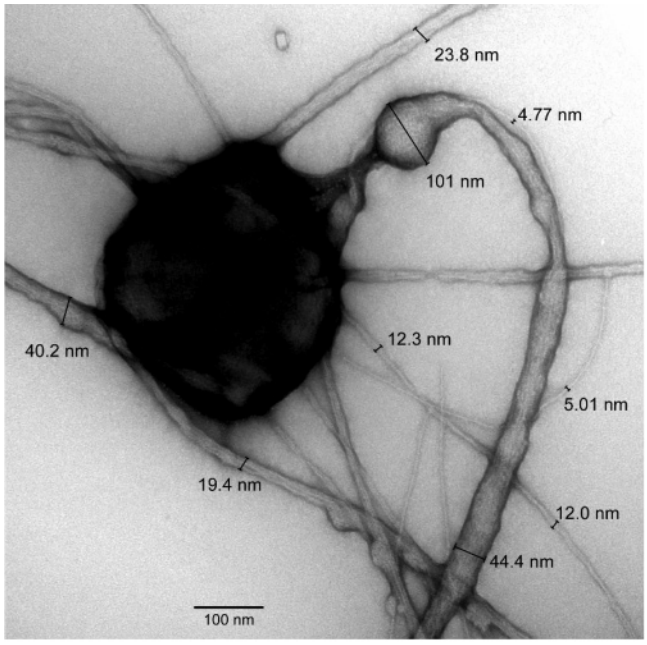

FIGURE 2: Representative HD fibrils of HaPrP23−144 grown in 10 mM HEPES (pH 7.5). The fibrils are characteristically bundled and display a wide range of diameters. Individual strands measured ~5 nm in diameter with bundles ranging in size from 2 to 9 times larger.

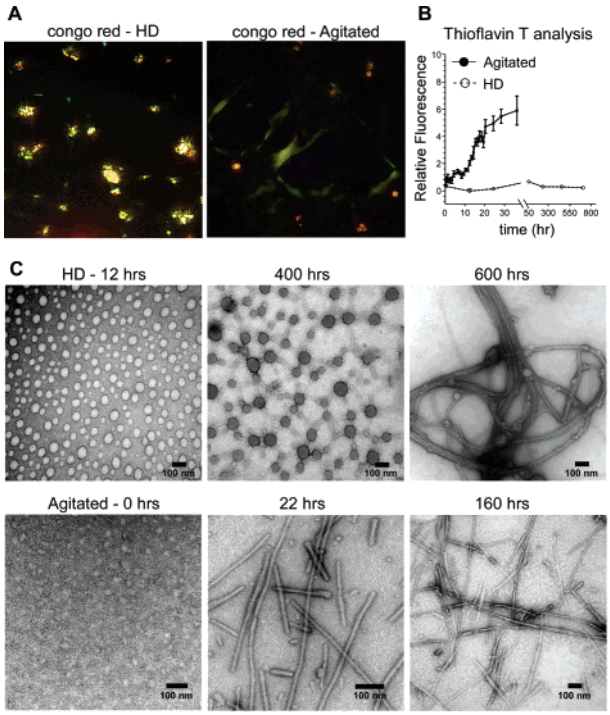

FIGURE 3: HaPrP23−144 fibrils in a HD environment form more slowly and differ ultrastructurally from those formed with agitation. A sample of HaPrP23−144 incubated in 10 mM Bis-Tris propane was subjected to either agitation at 1000 rpm or incubation without agitation in HDs. (A) Both reaction mixtures displayed apple-green birefringence when incubated with Congo Red. (B) ThT curves for HaPrP23−144 fibrillization. Agitated reaction mixtures were more responsive to ThT than the HD fibrils. Error bars are expressed as the standard error of the mean for $N = 3$. (C) TEM time course for HD and agitated fibrillization reactions. No fibrils were present early in the reaction. Within 22 h, mature fibrils were present in the agitated reaction mixtures. In the HD reaction, globules were present by 12 h and displayed networking properties by 400 h and mature fibrils by 600 h.

harsh denaturants, we consistently observed globules (here simply defined as a spherical mass) that were unusually large and reminiscent of detergent micelles (e.g., Figure 1A).

To ensure that globule formation in the HDs was not an artifact of detergent carryover from the bacterial lysis, we also purified the peptide without detergent lysis according to the method of Zahn et al. (*25*). When HaPrP23−144 was purified without detergents (BugBuster, EMD Biosciences), then placed into HDs, and analyzed by TEM, large globules were still observed (Figure 1B of the Supporting Information), thus demonstrating that they were not detergent micelles. Given that the globules were not observed in reaction mixtures containing only vector or buffer, the spherical structures must represent large peptide assemblies composed of HaPrP23−144 and buffer.

The supramolecular spherical structures were formed at neutral to basic pH in a variety of dilute buffers (Figure 1B−E) and with repeated preparations of HaPrP23−144. Importantly, they were far larger than most previous reports of soluble oligomers, ranging from a few nanometers to 1 μm or more in diameter (Figure 1). Surprisingly, many of them appeared to be interconnected with fibrillar material (e.g., Figure 1B−E), suggesting a direct association between the two and a potential intermediary role for the large peptide assemblies. When HaPrP23−144 was agitated in microfuge tubes, globules such as those shown in Figure 1 were not observed (Figure 3C, bottom panels), nor were they observed in microfuge tubes without agitation (data not shown). These data suggested that the globules were specific to the HD environment.

Atypical Fibrils Are Formed in Reaction Mixtures Containing Supramolecular Globules. The large spherical HaPrP23−144 assemblies were usually associated with fibrils displaying variable morphologies, as shown in Figure 1. Despite the diversity of the HD fibrils, some general characteristics were observed. They were typically entangled, highly curved, and bundled with extensive bifurcation (Figure 1F−I). These fibrils were nevertheless consistent with previous microscopic descriptions of general amyloid morphology in that individual strand diameters within the bundles ranged in diameter from 3 to 8 nm (Figure 2, and Figure 3 of the Supporting Information) (*26*−*29*), and they demonstrated apple-green birefringence when stained with Congo Red (Figure 3A). Thus, the HD environment promoted the formation of morphologically diverse amyloid-like fibrils which were, in many instances, reminiscent of the tangled plaques observed in vivo (*27*).

Peptide Globules Precede Fibril Formation in the HD Environment. We next asked whether the supramolecular assemblies preceded the unusual fibrils or if both types of structures formed concurrently. After ultracentrifugation of the sample to remove any aggregates that might interfere with the assay, the kinetics of HD and agitated reactions were monitored using thioflavin T (ThT) and TEM. Agitation of HaPrP23−144 gave a fibrillization curve with a lag phase of ~10 h followed by a log phase of fibril growth (Figure 3B). To our surprise, the ThT assay was much less sensitive for HD fibrillizations even though the buffer conditions were similar, and it was not possible to derive a kinetic curve from these data (Figure 3B). This lower ThT reactivity may be at least partly due to the smaller amount of fibrillar material

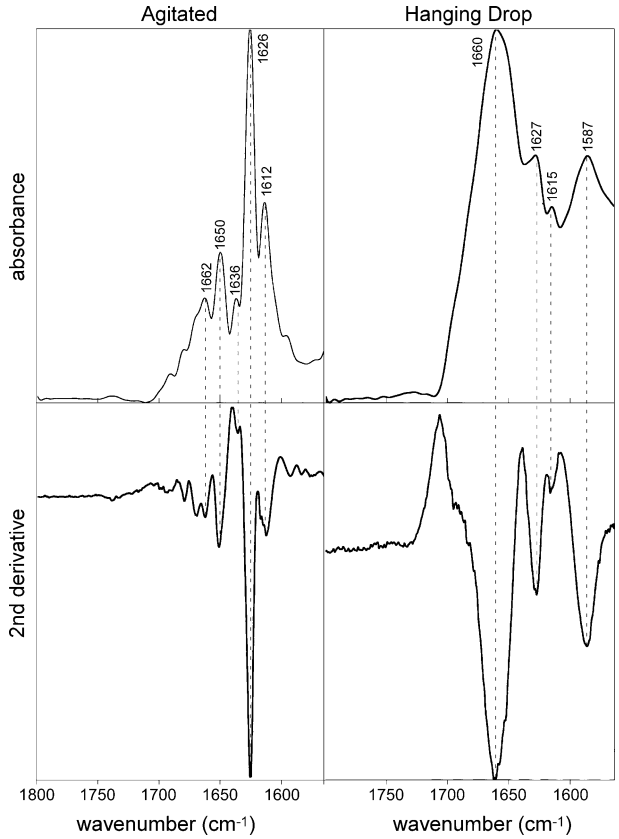

FIGURE 4: Attenuated total reflectance infrared spectroscopy (ATR-FTIR) of reaction products from HD and agitated reaction conditions show differences in secondary structure. Deconvoluted primary spectra (top) are aligned with their second derivatives (bottom). The HD reaction shows a greater variety of isoforms containing turn and loop structure (1650−1700 cm^{-1}), while the agitated fibrils show a greater proportion of β-sheet structure at 1627 cm^{-1}. The band at 1587 cm^{-1} is present in the HD reaction but not in any portion of the agitated reaction of the same sample.

formed in the hanging drop reactions when compared to agitated reactions (∼20% vs ∼80%). Therefore, reaction kinetics were estimated by TEM (Figure 3C). The TEM images confirmed that no fibrils were present at initial time points in either reaction. Consistent with the ThT data, the agitated reaction formed amyloid in ≤22 h and was complete within 160 h (Figure 3C, bottom panel). By contrast, the HD reaction was significantly slower, and the appearance of supramolecular peptide spheres clearly preceded fibril formation (Figure 3C, compare HD 12 h with HD 400 h). Within 600 h, characteristic fibrillar bundles were observed (Figure 3C, top, last panel) in the HD reaction mixture. Thus, hanging drop fibrillizations exhibited reaction kinetics slower than those of agitated fibrillizations, and the fibrils were preceded by the formation of supramolecular peptide globules.

Different Secondary Structures Are Present in HD and Agitated Fibrillization Reactions. The striking morphologies observed in the HD fibrils prompted us to question whether these fibrils were also unique at the molecular level. When precise structures are impossible to obtain from X-ray diffraction patterns or NMR, as is the case with heterogeneous amyloid aggregates, then Fourier transform infrared spectroscopy (FTIR) is considered a method of choice for examining changes in protein secondary structure (*30*). Consequently, differences in secondary structure between the

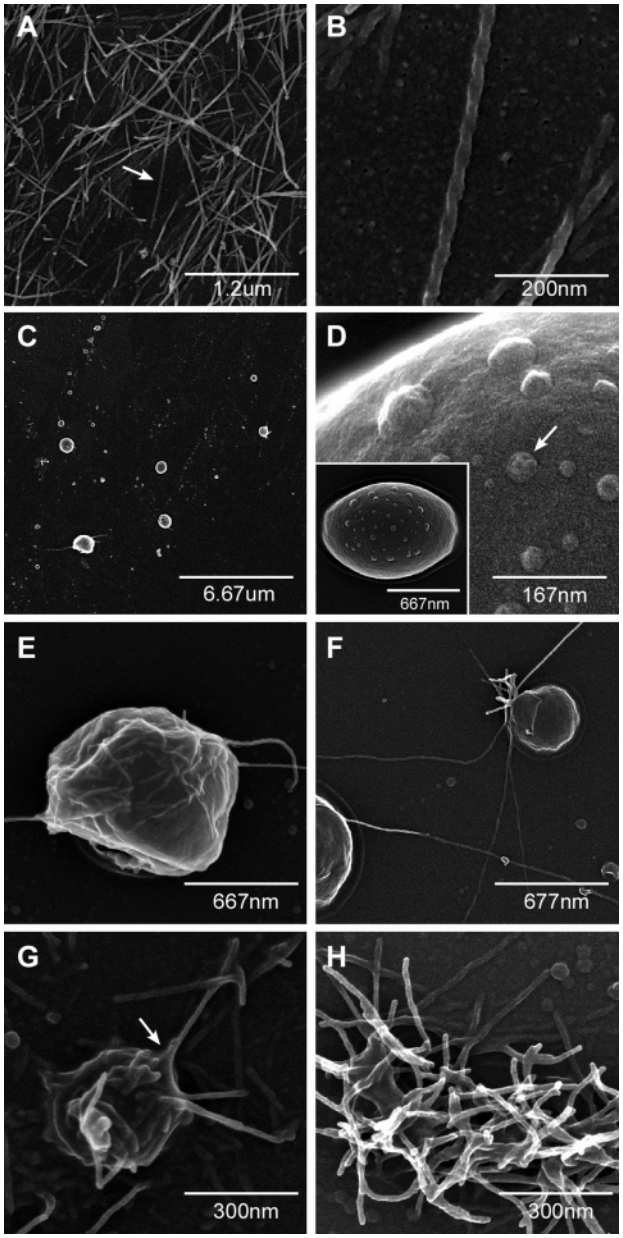

FIGURE 5: Supramolecular globules extrude HaPrP23−144 fibrils. SEM images of agitated (A and B) and hanging drop (C−H) fibrillization reaction mixtures. (A) HaPrP23−144 agitated in 10 mM Bis-Tris propane (pH 7). The arrow indicates the fibril bundle shown in panel B which has characteristic curvilinear and helical fibrillar morphology. (C) HD with HaPrP23−144 in 10 mM Bis-Tris propane (pH 7). The relative sizes and ultrastructural characteristics observed by SEM are consistent with images obtained by TEM analysis (see Figure 1). (D) Representative globules with surface features (arrow) ranging in size from ∼20 to 70 nm. The inset shows the entire assembly. (E and F) Active fibrillization associated with supramolecular peptide globules. (G) Fibrils extrude from and appear to be contiguous with the globule (arrow). (H) Mature HD fibrils are highly entangled and bundled.

two types of reaction products were examined by FTIR. Agitated HaPrP23−144 fibrils routinely displayed significant β-sheet character with a major band at 1626 cm^{-1}, as expected from amyloid, in addition to minor bands typical of α-helical and turn structures at 1653 and 1663/1670 cm^{-1}, respectively (Figure 4, left panels). By contrast, the HD mixture was more complex, distinguished by a broad band between 1650 and 1700 cm^{-1}, which likely represented a mixture of incompletely resolved random coil, α-helix, turn,

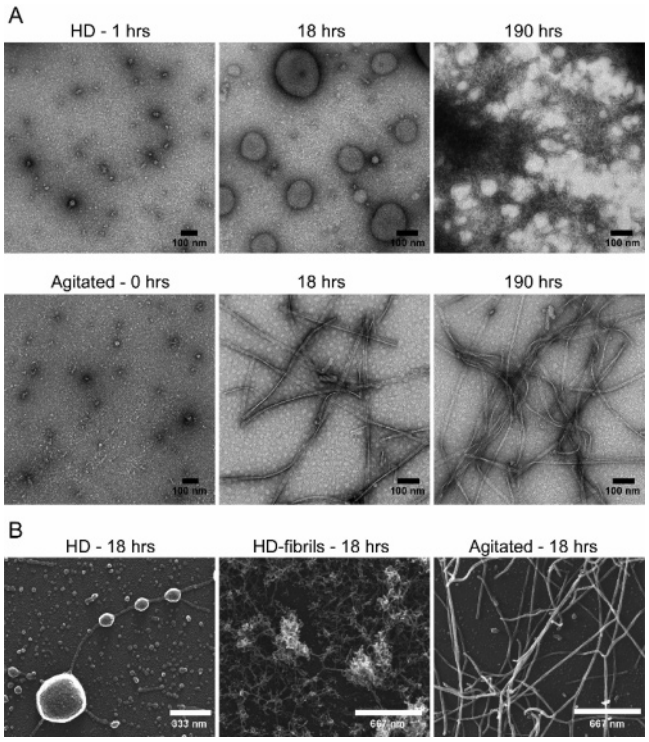

FIGURE 6: Aβ40 peptide forms supramolecular globules in the HD environment. A sample of Aβ40 incubated in 25 mM MES (pH 5.4) was subjected to either agitation at 600 rpm or incubation in HDs and analyzed. (A) TEM analysis of Aβ40 fibrillization reactions. After incubation for 1 h, both reaction mixtures displayed soluble oligomers and small protofibrils but no mature fibrils. By 18 h, the HD reaction mixture exhibited numerous examples of globules while the agitated reaction mixture was essentially complete. By 190 h, both reactions produced fibrillar material. (B) SEM analysis of Aβ40 fibrillization reactions. In the HD reactions at 18 h, examples of both globules and mature fibrils could be found on the same chip. In many instances, globules were interconnected by polymerized Aβ40 (left panel). At 18 h, both HD and agitated reaction mixtures had mature fibrils, although in the HD reaction mixture the fibrils were more bundled and interconnected.

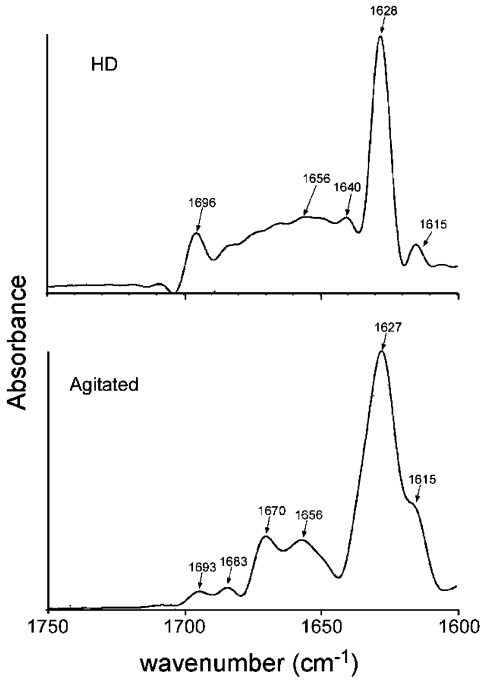

FIGURE 7: Attenuated total reflectance infrared spectroscopy (ATR-FTIR) of Aβ40 fibrils. Fibrillar material from HD and agitated reaction mixtures was pelleted and analyzed by FTIR. Analysis of deconvoluted primary spectra reveals structural differences in agitated vs HD fibrils. Both types of fibrils show significant β-sheet character, but the HD fibrils appear to display a greater variety of isoforms in the 1656−1696 cm^{-1} region.

and loop structures, as well as a characteristic β-sheet band at 1627 cm^{-1} (Figure 4, right panels). Additionally, we observed a peak at 1587 cm^{-1} in both the primary and secondary derivative spectra (Figure 4, right panels), which we were unable to associate with any known protein structure. The 1587 cm^{-1} band was not observed in the spectra of the agitated fibrils of the same peptide sample, increasing the likelihood that it was specific to the HD reaction rather than the result of a nonprotein impurity. Overall, the infrared spectra supported the hypothesis that there were structural differences in the products formed in quiescent versus agitated fibrillization reactions.

Supramolecular Peptide Globules Are Contiguous with Growing Fibrils. While the TEM data strongly suggested that the fibrils could be extruded directly from the globules (e.g., Figure 1B−F, and Figure 3A of the Supporting Information), there were other instances in which fibrils and globules may have been coincidentally associated (e.g., in Figure 2, note the fibrils running underneath the globule). Scanning electron microscopy (SEM) of progressing HD fibrillizations was used to further probe whether fibrils emanated from the large globules. SEM of the agitated fibrils displayed extensive networks, often with a helical topography (Figure 5A,B). After 350 h, the HD fibrillizations again revealed peptide globules, some of which were studded with spherical structures (Figure 5D). Maturing fibrils appeared to be contiguous with many of the peptide globules (Figure 5E−G, arrow) displaying morphologies which were consistent with numerous TEM observations. Entanglements of thickly bundled, curved fibrils were also observed on different locations of the same chip (Figure 5H). Thus, the SEM images further support the idea that complex fibrillar networks emanate directly from the globular formations.

Formation of Supramolecular Peptide Spheres by Aβ40. To determine whether other amyloid-forming peptides could also form fibrils via similar supramolecular peptide globules, Aβ40 was suspended in HDs. Similar phase partitioning of Aβ40 into large spherical structures was observed at pH 5.4, near the isoelectric point of the peptide (Figure 6A, top panels). As with HaPrP23−144, the Aβ40 peptide formed large globules only in the HD environment. No such structures were observed under agitated conditions even though similar buffer conditions were used (Figure 6A, bottom panels). Further analysis of the Aβ40 HD reaction by SEM suggested that fibrils were associated with and directly extruded from the globules (Figure 6B) in a manner similar to that seen in the HaPrP23−144 HD reaction (Figure 5). Finally, FTIR analysis of the Aβ40 HD and agitated reactions showed that there were subtle but reproducible structural differences between the agitated and quiescent fibrils (Figure 7). Overall, our results suggest that supramolecular peptide spheres represent intermediary components of a reaction mechanism that can yield distinctive amyloid products.

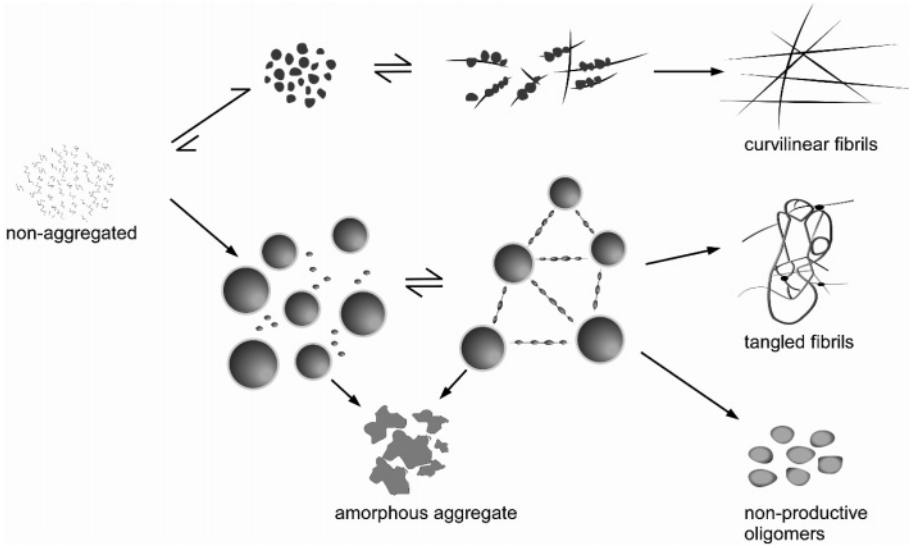

FIGURE 8: Model of amyloid formation in the HD environment. In the top scheme, agitation prompts the efficient formation of amyloid fibrils via formation of small soluble oligomers which then interact to form fibrils. In our hands, approximately 80% of the input peptide was pelleted fibrillar material. In the bottom scheme, hanging drop conditions prompt the formation of supramolecular multimeric assemblies which eventually interconnect and progress into highly bundled amyloid fibrils. When compared to agitated reactions, HD reactions proceed through a more diverse set of intermediates and yield more heterogeneous amyloid products. In some instances, HaPrP23−144 also formed amorphous aggregates and apparently inert globular species. We estimate that approximately 20% of the original peptide formed fibrillar material within the time frame of our HD studies (see Experimental Procedures).

DISCUSSION

Our data clearly show that the pathway of peptide self-assembly can be profoundly altered by simply changing the physical reaction environment, while the resulting differences in morphology and secondary structure between the two types of fibrils are indicative of fundamental changes in the fibrillization mechanism. Within the static environment of the hanging drop, this mechanism involves oligomeric species much larger than those that are typically described. Fibril formation via these supramolecular peptide spheres was consistently observed in multiple independent purifications and subsequent hanging drop preparations of HaPrP23−144. Thus, it does not appear to constitute an off-pathway mechanism of fibril formation within the hanging drop environment but rather the primary one.

HaPrP23−144 and Aβ40 are amphipathic peptides containing a short but hydrophobic C-terminus and a hydrophilic N-terminus, as shown graphically with a Kyte−Doolittle hydropathy plot (*31*) in Figure 2 of the Supporting Information. These properties could allow them to self-assemble into structures resembling detergent micelles under the right conditions. In fact, peptide micelles have been described for some amyloidogenic peptides, including Aβ42 (*32*), which has a hydrophobicity profile similar to that of HaPrP23−144. The HD environment appears to promote these ultrastructural features, perhaps by providing an increased polar air−water interface area. The hydrophobic surface area at the air−water interface has been described as an important variable in protein aggregation and fibrillization (*33*). Since the majority of amino acids in HaPrP23−144 are hydrophilic, these residues may partition away from this hydrophobic surface into the aqueous core of the globule, thus promoting phase separation and eventual self-aggregation. The SEM images support the notion that over time fibrillization-competent nuclei originating on the globular surface (e.g., Figure 5D) could polymerize into entangled networks of highly bundled fibrils (e.g., Figure 5H). Thus, the process of fibril extrusion from such globules would still be consistent with nucleation-dependent polymerization, albeit with slower reaction kinetics and more structural heterogeneity in the prefibrillar species. Agitation would promote more rapid fibrillization by providing kinetic energy to the reaction system and dissociating larger aggregates into smaller particles (*34*).

The high degree of bundling observed in the hanging drop environment may also help to explain the diminished ThT fluorescence. Such a decrease has been observed in other instances in which fibrils have aggregated into densely matted assemblies (*4*). We also noticed that, although HaPrP23−144 reacted with ThT, it was much less responsive than corresponding reaction mixtures containing similar concentrations of Aβ40 fibrils (unpublished observations). It may be that the positively charged ThT interacts less vigorously with peptides such as HaPrP23−144, which at most pH values is positively charged due to its abnormally high isoelectric point (pI = 11.2). In a mechanistic study of ThT, Khurana and co-workers discussed a similarly cationic peptide (KLEG, KLKLKLELELELG) that formed fibrils but failed to elicit ThT fluorescence (*35*). The cumulative effects of the high degree of bundling coupled with the smaller amounts of fibrillar material produced (see Results) and the positive charge of the peptide may lead to the poor ThT reactivity observed with the hanging drop reactions.

Polymerization of HaPrP23−144 in the hanging drop environment appeared to occur outward from the globule (e.g., Figure 5E−G), suggesting that only the ends of the fibril were actively polymerizing. However, there were also many examples of large globules which appeared to be directly interacting with mature fibrils (e.g., Figures 1D and 2) and, in some cases, actually extruding a new fibril onto the mature fibril (Figure 1D). This suggests that new fibril

growth can occur along the length of an already mature fibril and could help explain why large fibril bundles were formed under HD conditions. In these instances, we postulate that the mature fibrils act as a scaffolding to promote new fibril growth.

In our model, the large globules form and then thermodynamically partition into either amorphous precipitate, inert material, or polymerization competent species yielding complex fibrillar networks (Figure 8). Such a heterogeneous mixture may in part explain the gross differences in the secondary structure of the HD reaction products when compared to agitated fibrils. While both reaction mixtures displayed the characteristic β-sheet associated with mature fibrils, HD mixtures also displayed a broader band from 1650 to 1700 cm^{-1} which likely represents a soluble mixture of partially structured conformers, only some of which were fibrillization competent. In the HD reactions, there was also a peak at 1587 cm^{-1}, an undefined region between the amide I and II bands where proteins most strongly absorb. This feature was not observed in the same peptide sample under agitated conditions, nor was it seen in the Aβ40 fibrillization reactions. Thus, it may represent unique secondary structural changes in one or more components of the HaPrP23−144 reaction mixture. One intriguing possibility is that this band represents α-pleated sheet secondary structure, first postulated by Linus Pauling in 1951 (*36*) and recently proposed as a prefibrillar intermediate in amyloid disease (*37*).

Previous reports have suggested that supramolecular aggregates derived from amyloidogenic peptides might give rise to fibrils (*38*, *39*), and Aβ "globulomers" reminiscent of the globules described here have been observed in vivo (*40*). Our data clearly illustrate a potential intermediary function for such unusually large multimeric peptide assemblies. The role that such large globular peptide species may play in amyloid-associated disease is not yet fully understood. Association of HaPrP23−144 and Aβ40 into globules is reminiscent of crystallography experiments in which "microdroplets" form due to intermolecular interactions prompted by abnormally high protein concentrations in the hanging drops. In fact, many amyloidoses are also prompted by abnormally high peptide concentrations (e.g., β_2-microglobulin in hemodialysis patients), resulting in fibrillar bundles deposited in tissues over months or years. Formation of tangled plaquelike fibrils under thermodynamic rather than kinetic control in the polar hydrophobic hanging drop environment could be analogous to the protein oligomerization across or between cell membranes which may constitute a critical aspect of the pathology observed in diseases of protein deposition.

ACKNOWLEDGMENT

We thank Drs. Byron Caughey, David Kocisko, and Bruce Chesebro for critical reading of the manuscript, Anita Mora for help with graphics, and Dr. Dave Dorward for technical assistance in obtaining images with the polarizing microscope. We declare no competing financial interest.

SUPPORTING INFORMATION AVAILABLE

Three supporting figures referenced in the main text illustrate the lack of fibril formation using a mock peptide purification in which an empty vector was transformed into *E. coli*, the Kyte−Doolittle hydropathy plot for HaPrP23−144 and Aβ40, and representative nonagitated fibril morphologies. This material is available free of charge via the Internet at http://pubs.acs.org.

REFERENCES

1. Merlini, G., and Bellotti, V. (2003) Molecular mechanisms of amyloidosis, *N. Engl. J. Med. 349*, 583−596.
2. Zerovnik, E. (2002) Amyloid-fibril formation. Proposed mechanisms and relevance to conformational disease, *Eur. J. Biochem. 269*, 3362−3371.
3. Surewicz, W. K., Jones, E. M., and Apetri, A. C. (2006) The emerging principles of mammalian prion propagation and transmissibility barriers: Insight from studies in vitro, *Acc. Chem. Res. 39*, 654−662.
4. Nilsson, M. R. (2004) Techniques to study amyloid fibril formation in vitro, *Methods 34*, 151−160.
5. Baskakov, I. V., Legname, G., Baldwin, M. A., Prusiner, S. B., and Cohen, F. E. (2002) Pathway complexity of prion protein assembly into amyloid, *J. Biol. Chem. 277*, 21140−21148.
6. Yamin, G., Uversky, V. N., and Fink, A. L. (2003) Nitration inhibits fibrillation of human α-synuclein in vitro by formation of soluble oligomers, *FEBS Lett. 542*, 147−152.
7. Collins, S. R., Douglass, A., Vale, R. D., and Weissman, J. S. (2004) Mechanism of prion propagation: Amyloid growth occurs by monomer addition, *PLoS Biol. 2*, e321.
8. Kayed, R., Head, E., Thompson, J. L., McIntire, T. M., Milton, S. C., Cotman, C. W., and Glabe, C. G. (2003) Common structure of soluble amyloid oligomers implies common mechanism of pathogenesis, *Science 300*, 486−489.
9. Kirkitadze, M. D., Bitan, G., and Teplow, D. B. (2002) Paradigm shifts in Alzheimer's disease and other neurodegenerative disorders: The emerging role of oligomeric assemblies, *J. Neurosci. Res. 69*, 567−577.
10. Bitan, G., Fradinger, E. A., Spring, S. M., and Teplow, D. B. (2005) Neurotoxic protein oligomers: What you see is not always what you get, *Amyloid 12*, 88−95.
11. Cleary, J. P., Walsh, D. M., Hofmeister, J. J., Shankar, G. M., Kuskowski, M. A., Selkoe, D. J., and Ashe, K. H. (2005) Natural oligomers of the amyloid-β protein specifically disrupt cognitive function, *Nat. Neurosci. 8*, 79−84.
12. Souillac, P. O., Uversky, V. N., and Fink, A. L. (2003) Structural transformations of oligomeric intermediates in the fibrillation of the immunoglobulin light chain LEN, *Biochemistry 42*, 8094−8104.
13. Walsh, D. M., Hartley, D. M., Kusumoto, Y., Fezoui, Y., Condron, M. M., Lomakin, A., Benedek, G. B., Selkoe, D. J., and Teplow, D. B. (1999) Amyloid β-protein fibrillogenesis. Structure and biological activity of protofibrillar intermediates, *J. Biol. Chem. 274*, 25945−25952.
14. Kayed, R., Sokolov, Y., Edmonds, B., McIntire, T. M., Milton, S. C., Hall, J. E., and Glabe, C. G. (2004) Permeabilization of lipid bilayers is a common conformation-dependent activity of soluble amyloid oligomers in protein misfolding diseases, *J. Biol. Chem. 279*, 46363−46366.
15. Lashuel, H. A., Hartley, D., Petre, B. M., Walz, T., and Lansbury, P. T., Jr. (2002) Neurodegenerative disease: Amyloid pores from pathogenic mutations, *Nature 418*, 291.
16. Demuro, A., Mina, E., Kayed, R., Milton, S. C., Parker, I., and Glabe, C. G. (2005) Calcium dysregulation and membrane disruption as a ubiquitous neurotoxic mechanism of soluble amyloid oligomers, *J. Biol. Chem. 280*, 17294−17300.
17. Zhu, M., Han, S., Zhou, F., Carter, S. A., and Fink, A. L. (2004) Annular oligomeric amyloid intermediates observed by in situ atomic force microscopy, *J. Biol. Chem. 279*, 24452−24459.
18. Catharino, S., Buchner, J., and Walter, S. (2005) Characterization of oligomeric species in the fibrillization pathway of the yeast prion Ure2p, *Biol. Chem. 386*, 633−641.
19. Dong, J., Apkarian, R. P., and Lynn, D. G. (2005) Imaging amyloid β peptide oligomeric particles in solution, *Bioorg. Med. Chem. 13*, 5213−5217.
20. Mastrangelo, I. A., Ahmed, M., Sato, T., Liu, W., Wang, C., Hough, P., and Smith, S. O. (2006) High-resolution atomic force microscopy of soluble Aβ42 oligomers, *J. Mol. Biol. 358*, 106−119.

21. Petkova, A. T., Leapman, R. D., Guo, Z., Yau, W. M., Mattson, M. P., and Tycko, R. (2005) Self-propagating, molecular-level polymorphism in Alzheimer's β-amyloid fibrils, *Science 307*, 262−265.
22. Colucci, M., Moleres, F. J., Xie, Z. L., Ray-Chaudhury, A., Gutti, S., Butefisch, C. M., Cervenakova, L., Wang, W., Goldfarb, L. G., Kong, Q., Ghetti, B., Chen, S. G., and Gambetti, P. (2006) Gerstmann-Straussler-Scheinker: A new phenotype with 'curly' PrP deposits, *J. Neuropathol. Exp. Neurol. 65*, 642−651.
23. Ghetti, B., Piccardo, P., Spillantini, M. G., Ichimiya, Y., Porro, M., Perini, F., Kitamoto, T., Tateishi, J., Seiler, C., Frangione, B., Bugiani, O., Giaccone, G., Prelli, F., Goedert, M., Dlouhy, S. R., and Tagliavini, F. (1996) Vascular variant of prion protein cerebral amyloidosis with τ-positive neurofibrillary tangles: The phenotype of the stop codon 145 mutation in PRNP, *Proc. Natl. Acad. Sci. U.S.A. 93*, 744−748.
24. Moore, R. A., Herzog, C., Errett, J., Kocisko, D. A., Arnold, K. M., Hayes, S. F., and Priola, S. A. (2006) Octapeptide repeat insertions increase the rate of protease-resistant prion protein formation, *Protein Sci. 15*, 609−619.
25. Zahn, R., von Schroetter, C., and Wuthrich, K. (1997) Human prion proteins expressed in *Escherichia coli* and purified by high-affinity column refolding, *FEBS Lett. 417*, 400−404.
26. Rochet, J. C., and Lansbury, P. T., Jr. (2000) Amyloid fibrillogenesis: Themes and variations, *Curr. Opin. Struct. Biol. 10*, 60−68.
27. Sipe, J. D., and Cohen, A. S. (2000) Review: History of the amyloid fibril, *J. Struct. Biol. 130*, 88−98.
28. Serpell, L. C., Sunde, M., and Blake, C. C. (1997) The molecular basis of amyloidosis, *Cell. Mol. Life Sci. 53*, 871−887.
29. Sipe, J. D. (1992) Amyloidosis, *Annu. Rev. Biochem. 61*, 947−975.
30. Seshadri, S., Khurana, R., and Fink, A. L. (1999) Fourier transform infrared spectroscopy in analysis of protein deposits, *Methods Enzymol. 309*, 559−576.
31. Kyte, J., and Doolittle, R. F. (1982) A simple method for displaying the hydropathic character of a protein, *J. Mol. Biol. 157*, 105−132.
32. Soreghan, B., Kosmoski, J., and Glabe, C. (1994) Surfactant properties of Alzheimer's Aβ peptides and the mechanism of amyloid aggregation, *J. Biol. Chem. 269*, 28551−28554.
33. Sluzky, V., Tamada, J. A., Klibanov, A. M., and Langer, R. (1991) Kinetics of insulin aggregation in aqueous solutions upon agitation in the presence of hydrophobic surfaces, *Proc. Natl. Acad. Sci. U.S.A. 88*, 9377−9381.
34. Serio, T. R., Cashikar, A. G., Kowal, A. S., Sawicki, G. J., Moslehi, J. J., Serpell, L., Arnsdorf, M. F., and Lindquist, S. L. (2000) Nucleated conformational conversion and the replication of conformational information by a prion determinant, *Science 289*, 1317−1321.
35. Khurana, R., Coleman, C., Ionescu-Zanetti, C., Carter, S. A., Krishna, V., Grover, R. K., Roy, R., and Singh, S. (2005) Mechanism of thioflavin T binding to amyloid fibrils, *J. Struct. Biol. 151*, 229−238.
36. Pauling, L., and Corey, R. B. (1951) The pleated sheet, a new layer configuration of polypeptide chains, *Proc. Natl. Acad. Sci. U.S.A. 37*, 251−256.
37. Daggett, V. (2006) α-Sheet: The Toxic Conformer in Amyloid Diseases? *Acc. Chem. Res. 39*, 594−602.
38. Westlind-Danielsson, A., and Arnerup, G. (2001) Spontaneous in vitro formation of supramolecular β-amyloid structures, "βamy balls", by β-amyloid 1−40 peptide, *Biochemistry 40*, 14736−14743.
39. Hamodrakas, S. J., Hoenger, A., and Iconomidou, V. A. (2004) Amyloid fibrillogenesis of silkmoth chorion protein peptide-analogues via a liquid-crystalline intermediate phase, *J. Struct. Biol. 145*, 226−235.
40. Barghorn, S., Nimmrich, V., Striebinger, A., Krantz, C., Keller, P., Janson, B., Bahr, M., Schmidt, M., Bitner, R. S., Harlan, J., Barlow, E., Ebert, U., and Hillen, H. (2005) Globular amyloid β-peptide oligomer: A homogenous and stable neuropathological protein in Alzheimer's disease, *J. Neurochem. 95*, 834−847.

BI700247Y